Measurements of Flow-Induced Anisotropic Thermal Conduction in a Polyisobutylene Melt Following Step Shear Flow

Venkat Balasubramanian, Kendall Bush, Stoyan Smoukov, David C. Venerus,* and Jay D. Schieber

Department of Chemical Engineering and Center of Excellence in Polymer Science and Engineering, Illinois Institute of Technology, Chicago, Illinois 60616

Received April 19, 2005; Revised Manuscript Received May 18, 2005

ABSTRACT: Flow-induced anisotropic thermal conduction in a polyisobutylene melt subjected to shear deformations is studied experimentally. Time-dependent measurements of the full (four components) thermal diffusivity tensor following step shear strain flow are presented. These data were obtained with a novel experimental setup based on the optical technique of forced Rayleigh scattering. Birefringence and stress measurements are made for the same flow, and the well-known stress−thermal rule is found to be satisfied. Thermal diffusivity data and stress data are used to test directly the stress−thermal rule, which is also satisfied for the two cases considered. Consideration of stress−thermal coefficients from the present and previous studies gives preliminary evidence that flow-induced anisotropic thermal conduction is a universal phenomenon for flexible polymers.

Introduction

Polymer processing flows such as fiber spinning, blow molding, and injection molding are common examples of processes where a flowing polymer liquid is solidified so that a final product with the desired shape and physical properties is produced. The external addition/removal of heat required by these operations combined with the dissipation of large amounts of energy makes polymer processing flows inherently nonisothermal.[1,2] In addition, it is well-known that polymer viscosity and relaxation time are strong functions of temperature. Hence, the flow of polymer liquids involves a complex interaction of mechanical and thermal transport processes.[3−5] The mechanical, or rheological, behavior of polymer liquids has been an active area of research for more than 50 years.[6,7] Research on thermodynamics and thermal transport in flowing polymers, while far behind rheology, has increased significantly over the past decade.[8−10]

A small body of theoretical work indicates that thermal conductivity is anisotropic in deforming polymer liquids.[11−13] For such systems, Fourier's law for the energy flux $\mathbf{q}$ is

$$\mathbf{q} = -\mathbf{k}\cdot\nabla T \tag{1}$$

where T is the temperature field and $\mathbf{k}$ is the thermal conductivity tensor. Using a simple network model for polymer liquids, van den Brule[11] suggested that the thermal conductivity tensor and extra stress tensor $\boldsymbol{\tau}$ are linearly related. This idea can be expressed as follows:

$$\mathbf{k} - \frac{1}{3}\mathrm{tr}(\mathbf{k})\boldsymbol{\delta} = k_{\mathrm{eq}}C_{\mathrm{t}}\left(\tau - \frac{1}{3}\mathrm{tr}(\boldsymbol{\tau})\right) \tag{2}$$

where k_{eq} is the equilibrium thermal conductivity and C_{t} is the stress−thermal coefficient.

The "stress−thermal rule" given in eq 2 is analogous to the well-known stress−optic rule[14,15] relating the refractive index tensor $\mathbf{n}$ to $\boldsymbol{\tau}$:

$$\mathbf{n} - \frac{1}{3}\mathrm{tr}(\mathbf{n})\boldsymbol{\delta} = C_{\mathrm{o}}\left(\tau - \frac{1}{3}\mathrm{tr}(\boldsymbol{\tau})\right) \tag{3}$$

where C_{o} is the stress−optic coefficient. The molecular basis for eq 3 is that anisotropies in the stress and refractive index tensors arise from the same measure of polymer chain segment orientation and that during flow the distribution of chain segments is Gaussian. The stress−optic rule has been found to be valid for a large number of polymer liquids, and numerous rheo-optical techniques have been developed to study the flow behavior of complex fluids.[14,15−19] For liquids composed of flexible polymers well above their glass transition temperature, violations of eq 3 appear to be limited to strong flows that are able to stretch polymer chains to an extent where the distribution of Kuhn segments becomes non-Gaussian.[15,18,19]

In a previous study, we reported the first quantitative measurements of anisotropic thermal conduction in a polymer liquid following a step shear deformation.[20,21] These results showed thermal conduction was enhanced in the flow direction and decreased in the vorticity direction, relative to the equilibrium level. Birefringence (anisotropy of the refractive index tensor) measured in the same flow allowed us, using a combination of eqs 2 and 3, to verify indirectly the stress−thermal rule for a polymer melt in shear flow.[20,21] In a similar study on a cross-linked polymer subjected to simple elongation,[22] we reported measurements of the thermal diffusivity tensor and tensile stress that provided direct evidence for the stress−thermal rule. Validity of the stress−thermal rule, eq 2, indicates that deformation-induced anisotropies in mechanical and thermal transport in polymers are governed by polymer chain orientation on a common length scale.[20−22] This observation could have profound implications on theoretical modeling because it provides guidance on the level of course graining necessary to describe anisotropic thermal conductivity. In addition, many of the results from molecular models of polymer dynamics to predict rheological behavior can, if eq 2 is generally valid, be immediately used to develop models for flow-induced anisotropic thermal conductivity.

In a recently published letter,[23] we reported the first measurements of the complete thermal diffusivity tensor in a polymer liquid subjected to step strain flow. Here, we present an expanded set of results and provide

* Corresponding author. E-mail: venerus@iit.edu.

10.1021/ma050827j CCC: $30.25
Published on Web 06/15/2005

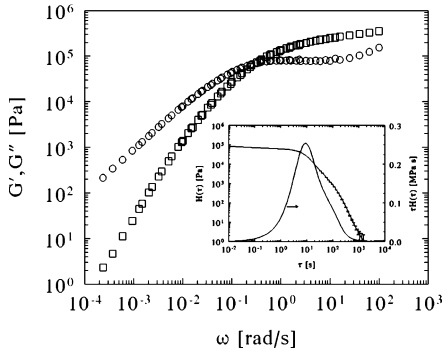

Figure 1. Dynamic modulus of PIB131K (M_w = 130.7 kDa) at 25 °C measured in small-amplitude oscillatory shear. The inset shows the continuous spectrum of relaxation times obtained from dynamic modulus data.

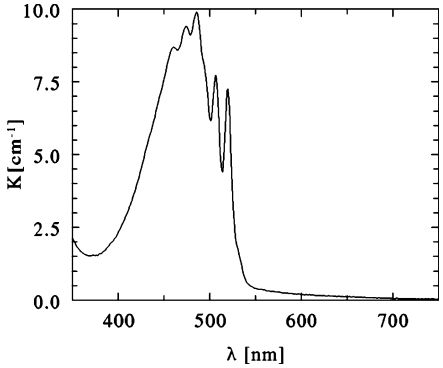

Figure 2. Absorption spectra for PIB131K containing 0.03% w/w qunizarin dye. The absorption coefficient for the FRS writing laser is K(514.5 nm) = 4.5 cm^{-1}.

the details of the novel experimental method used to obtain them. In addition to the thermal diffusivity data, we have obtained both birefringence and stress data in the same flow. The composite set of results is used to show that both the stress−optic and stress−thermal rules are valid. Implications of the present results and previous findings are discussed in an effort to identify the molecular origin of flow-induced anisotropic thermal conduction in macromolecules.

Experimental Section

Test Samples and Preparation. The test fluid is a polyisobutylene melt (Polymer Source Inc.) with a reported weight-average molecular weight M_w = 130.7 kDa and ratio of weight- to number-average molecular weight M_w/M_n = 1.24. Small-amplitude oscillatory shear measurements on this polyisobutylene (PIB131K) were conducted in parallel plate flow on a Rheometrics mechanical spectrometer (RMS-800) at temperatures of 25, 50, and 75 °C. The principle of time−temperature superposition was used to shift the data to a temperature of 25 °C to obtain the dynamic shear modulus data shown in Figure 1. The data in Figure 1 are typical for a moderately entangled polymer liquid[7] ($Z = M_w/M_e = 130.7/8 \simeq 16$ entanglements/chain). From these data we estimate the plateau modulus from the value of $G'(\omega)$ where $G''(\omega)$ goes through a minimum to obtain $G_N = 250 \pm 25$ kPa. The inset to Figure 1 shows the continuous spectrum of relaxation times $H(\tau)$ obtained from the dynamic modulus, which give a mean relaxation time $\tau_p \simeq 10$ s. A subtle shoulder in $H(\tau)$ at $\tau \simeq 100$ s indicates the presence of a high molecular weight tail in the molecular weight distribution of the PIB131K. An estimate of the longest Rouse relaxation time[7] τ_R (or time for stretched chains to relax to their equilibrium length) is $\tau_R = \tau_p/3Z \simeq 0.2$ s.

The FRS optical technique (described below) used to measure thermal diffusivity requires the test material to absorb radiation in a portion of the visible spectra. Since PIB is essentially transparent in the visible spectra (400−750 nm), trace amounts of a dye known as quinizarin (Sigma Aldrich) were uniformly dispersed within the polymer. This was achieved by first dissolving the dye and polymer in an excess amount of a volatile solvent (cyclohexane). The dye−polymer−solvent mixture was poured into a Petri dish, and the solvent was stripped off in a vacuum oven at 50 °C until the mass of the film was constant (several weeks). The absorption coefficient K vs wavelength λ for a typical PIB film containing 0.03% (w/w) quinizarin produced by this process is shown Figure 2. Portions of the dyed PIB film were transferred to the shear flow optical device (described below) and debubbled in a vacuum oven at 50 °C.

All rheo-optical and FRS experiments were conducted at a temperature of 25 ± 1 °C.

Rheo-Optical Measurements. Here we consider shear deformations with x_1 as the flow direction and x_2 as the gradient direction. If a shear strain γ is applied to an incompressible viscoelastic fluid, then the state of stress in the fluid is given by the shear stress τ_{12} and two normal stress differences $\tau_{11} - \tau_{22}$ and $\tau_{22} - \tau_{33}$.[6] For step strain flows of viscoelastic liquids, the following relationship between the shear stress and first normal stress difference known as the Lodge−Meissner relation[6,7] has been shown to be valid: $\tau_{11} - \tau_{22} = \gamma\tau_{12}$. Mechanical measurements of τ_{12} for $\gamma = 2.5$ were made using the cone and plate geometry on the RMS-800. The high modulus of the PIB 131K melt precluded attempts to measure $\tau_{11} - \tau_{22}$ (axial compliance) and to obtain τ_{12} at higher strains.

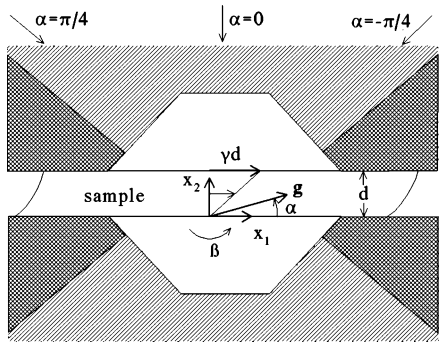

Figure 3. Schematic of shear flow optical device used for birefringence and FRS measurements showing shear flow coordinate system (x_1, x_2, x_3) and angles α and β that describe orientation of grating vector **g**.

A custom-made, shear flow optical device was used for birefringence and FRS measurements. Planar Couette flow is generated in the gap between a pair of opposed Dove prisms (70 mm × 50 mm × 25.4 mm) made of BK-7 glass. As shown schematically in Figure 3, one prism is stationary while the other moves parallel to the stationary prism. The stationary prism and moving prism, which is mounted on a pair of crossed roller bearings, are fixed to a rigid aluminum frame. Parallelism of the prism bases was established using an interferometric technique. The gap between the prism bases d can be adjusted using aluminum spacers over the range 0.5−1.5 mm. Motion of the moving prism was controlled using a stepper motor (K34HRFK-LNK-NS-00, Pacific Scientific) and driver (DPV 80001, Anaheim Automation) through a system of gears and lead screws. An LVDT (1000 HCA, Schaevitz Sensors) was used to measure the position of the moving plate. The stepper motor driver and LVDT were interfaced to a PC (PCI-MIO-16E-4, National Instruments) and controlled using a LabVIEW program. The time required to impose a shear strain is 80 ms $\ll \tau_R \ll \tau_p$ so that the flow is effectively a step strain deformation.[24] It should be noted that the stepper motor allows the shear flow optical device to achieve more precise deformation histories compared with our previous device,[20,21] which was driven by compressed springs. However, mechanical vibrations and the large electric field induced by the stepper motor prevented FRS measurements from being made until roughly 350 ms following the imposition of the step strain.

As shown in Figure 3, which shows the position of the prisms after a deformation has been imposed on the sample, optical paths with three different orientations α relative to the flow direction (x_1) are possible. Burghardt and co-workers[16,17] pioneered this type of configuration for measurement of the full refractive index tensor **n** in shear flows of polymer liquids. Here, we use a simple optical train consisting of the birefringent sample between crossed polarizers that allows the retardation δ to be obtained from the ratio of incident to transmitted intensity.[14,15] The birefringence is obtained from the retardation from the following: $\Delta n = \lambda^{\mathrm{HeNe}}\delta/2\pi d$, where $\lambda^{\mathrm{HeNe}} = 632.8$ nm. The relationship between the measured birefringence and refractive index tensor components in the shear flow coordinate system is given by

$$\Delta n = (n_{11} - n_{22})\cos^2(\alpha) + 2n_{12}\sin(\alpha)\cos(\alpha) + (n_{22} - n_{33}) \tag{4}$$

Hence, by making measurements of Δn for three values of α (= 0,π/4,−π/4), the quantities n_{12}, $n_{11} - n_{22}$, and $n_{22} - n_{33}$ can be obtained.

Forced Rayleigh Scattering (FRS). Flow-induced anisotropic thermal diffusivity measurements were made using an optical technique known as forced Rayleigh scattering.[25−27] The FRS technique can be simply described as the creation (writing) of an optical grating within the sample and monitoring (reading) the dynamic behavior of light diffracted by the grating. The grating is written by the intersection of two beams from a high-power Ar^+ laser (Innova 90C-A5, Coherent, Inc.) within a sample that partially absorbs ($Kd < 1$) at the wavelength ($\lambda^{Ar^+} = 514.5$ nm) of impinging light. The grating vector **g** lies in the plane formed by the two writing beams and is perpendicular to their direction of propagation. By a rapid, radiationless decay of the dye to its ground state, a sinusoidal temperature field is created with modulation amplitude δT and period $\Lambda = 2\pi/|\mathbf{g}| \simeq \lambda^{Ar^+}/\theta$ for $\theta \ll 1$, where θ is the intersection angle of the writing beams. Because the grating period Λ is much smaller than the spot size of the writing laser ($w = 1$ mm), the dynamics of the grating temperature field can be decoupled from the bulk temperature in the sample. Furthermore, if conditions for the plane grating approximation[25,27] are satisfied, δT following a pulse of the writing laser of duration t_p is governed by

$$\rho C_p \frac{d}{dt}\delta T = -\mathbf{g}\cdot\mathbf{k}\cdot\mathbf{g}\delta T \tag{5}$$

where ρ is the density and C_p is the specific heat. The solution of eq 5 can be written as

$$\delta T \propto \exp(-t/\tau_g) \tag{6}$$

where the grating relaxation time τ_g is given by

$$\tau_g = \frac{\Lambda^2}{4\pi^2\mathbf{g}\cdot\mathbf{D}\cdot\mathbf{g}} \tag{7}$$

where $\mathbf{D} = \mathbf{k}/\rho C_p$ is the thermal diffusivity tensor. For typical organic liquids and grating sizes used in this study, the grating relaxation time $\tau_g \sim 10^{-3}$ s. Hence, $\tau_g \ll \tau_p$, and the dynamics of the grating decay are completely decoupled from the relevant polymer chain dynamics.

Through a rapid thermophysical process, the sinusoidally modulated temperature field creates a sinusoidally modulated density field with amplitude $\delta\rho$. Since $c_0^2/g^2D^2 \ll 1$, where c_0 is the adiabatic speed of sound, $\delta\rho \propto \delta T$. Furthermore, since $\delta T \lesssim 10$ mK, $\delta n \propto \delta\rho$, so that from eq 6 we have $\delta n \propto \exp(-t/\tau_g)$. Dynamics of the grating are probed by a low-power HeNe laser (1135P, Uniphase) introduced at the Bragg angle. A photodetector (2001, New Focus) is used to measure the intensity of the first-order diffracted beam ($I_D \propto \delta n^2$) along with coherently ($\propto\sqrt{I_D}$) and incoherently scattered light producing a signal described by

$$V = A\exp(-2t/\tau_g) + B\exp(-t/\tau_g) + C \tag{8}$$

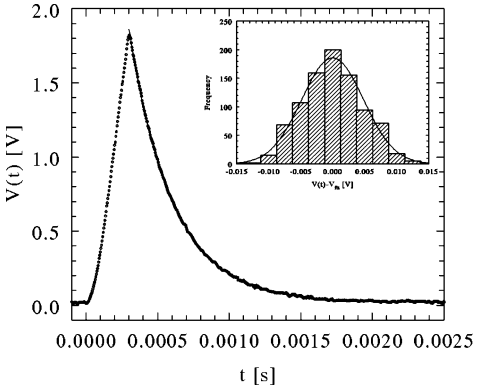

Figure 4. Typical photodetector voltage trace (symbols) from FRS experiment with $\Lambda = 40.4$ μm; $t_p = 0.3$. The solid line (for $t > t_p$) is a fit of eq 8 yielding $\tau_g = (5.94 \pm 0.12) \times 10^{-4}$ s. The inset shows a histogram of the residuals. This voltage trace was obtained 0.5 s following step strain flow of $\gamma = 2.5$ with $\alpha = \pi/4$ and $\beta = 0$.

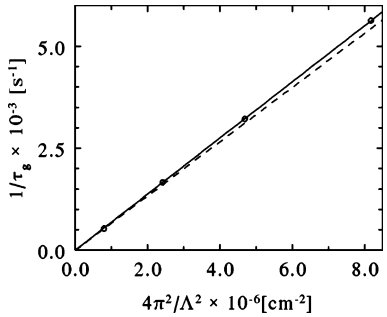

Figure 5. Typical isochronal plot showing dependence of grating relaxation time τ_g on grating period Λ (symbols). These values were obtained 0.5 s following step strain flow of $\gamma = 2.5$ with $\alpha = \pi/4$ and $\beta = 0$. The solid line through the symbols confirms eq 7 and the slope gives $\mathbf{g}\cdot\mathbf{D}\cdot\mathbf{g} = (D_{11} + 2D_{12} + D_{22})/2 = (6.88 \pm 0.06) \times 10^{-4}$ cm^2/s. The dashed line represents the equilibrium case.

A typical photodetector voltage trace is shown in Figure 4 for $\Lambda = 40.4$ μm, $t_p = 0.3$ ms, which shows the voltage from the photodetector both during and following the pulse of the writing laser. The Levenberg−Marquardt method used to fit eq 8 to V data for $t > t_p$ and determine τ_g is described elsewhere.[27] The inset to Figure 4 shows that the residuals have a Gaussian distribution. Consistency of the measured photodetector voltage with the biexponential function in eq 8 was carefully examined and interpreted as validation of the assumed thermophysical model.[23,27]

As an additional check of our FRS method, measurements are made at different grating sizes Λ in the range 25−75 μm to examine the dependence of τ_g on Λ. Figure 5 shows a typical isochronal ($t = 0.5$ s following the step strain) plot of $1/\tau_g$ vs $4\pi^2/\Lambda^2$ for $\gamma = 2.5$ with $\alpha = \pi/4$ and $\beta = 0$. It is clear from this figure that the dependence of τ_g on Λ is quadratic as required by eq 7. It should be noted that the uncertainties for $1/\tau_g$ and $4\pi^2/\Lambda^2$ are smaller than the symbols in Figure 5. The high correlation of the data with the expected linear relation is strong evidence that the assumed thermophysical model underlying the FRS technique is valid.[23,27] The slope of the solid line through the symbols in Figure 5 gives the thermal diffusivity at an angle of $\pi/4$ from the flow direction. As expected, the slope of this line deviates from the equilibrium value shown by the dashed line in Figure 5.

All reported thermal diffusivity values were obtained from independent FRS experiments made at four different grating sizes. For each grating size Λ, sample absorption coefficient K and writing laser pulse time t_p were optimized to maximize the signal-to-noise ratio for V while restricting bulk heating (<0.1 K).[21,27] The equilibrium value of thermal diffusivity for the PIB131K measured using FRS was found to be $D_{eq} = (6.65$

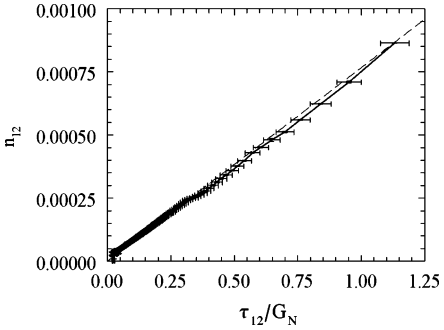

Figure 6. Birefringence n_{12} vs shear stress τ_{12} for PIB131K melt following step strain flow of $\gamma = 2.5$ (solid curve). Consistency with dashed line confirms the stress−optic rule and yields a stress−optic coefficient $C_o = (3.07 \pm 0.03) \times 10^{-9}$ Pa^{-1}.

$\pm 0.05) \times 10^{-4}$ cm^2/s. This value is consistent with the value found for the broad molecular weight distribution polyisobutylene (PIB85K) considered in a previous study.[21,27]

Following a step strain, the prisms were aligned creating different optical paths for the writing and reading laser beams. This allowed the grating vector to take four different orientations with respect to the coordinate system used to define the flow so that different projections of the thermal diffusivity tensor could be sampled with the FRS technique. The relationship between the thermal diffusivity measured along the grating direction $\mathbf{g}\cdot\mathbf{D}\cdot\mathbf{g}$ and the components of the thermal diffusivity tensor $D_{ij} = k_{ij}/\rho C_p$ in the shear flow coordinate system is given by[24]

$$\mathbf{g}\cdot\mathbf{D}\cdot\mathbf{g} = D_{11}\cos^2(\alpha)\cos^2(\beta) + 2D_{12}\sin(\alpha)\cos(\alpha)\cos^2(\beta) + D_{22}\sin^2(\alpha)\cos^2(\beta) + D_{33}\sin^2(\beta) \quad (9)$$

where α and β are angles between the grating vector $\mathbf{g}$ and the $x_1 - x_3$ and $x_1 - x_2$ planes, respectively, as shown in Figure 3. In previous work[20,21] we were restricted to the case $\alpha = 0$ so that D_{11} was obtained with $\beta = 0$ and D_{33} with $\beta = \pi/2$. In the present study, we also consider cases where $\beta = 0$ and $\alpha = \pm\pi/4$ that allow us to determine D_{22} and D_{12}.

Grating size Λ is changed by simply changing θ, the angle of intersection of the writing beams. Measurements of Λ are made by projecting magnified (20× microscope objective) images of the grating and a Ronchi slide (etched glass with 25 μm/line) on a CCD camera (2112, Silicon Video). Digitized images were analyzed allowing Λ to be determined with a high degree of accuracy (±0.05%). However, fluctuations in Λ of roughly ±0.5% were observed over the time of a typical experiment. For $\alpha = \pm\pi/4$, the small correction to the measured grating size to account for refraction at the prism−sample interface was taken into account.

Results and Discussion

The well-known stress−optic rule has been used extensively to study flow-induced orientation of polymeric liquids.[14,15] Here, we use birefringence measurements to augment mechanical measurements of the stress and to examine the possibility of slip at the sample−prism interface. The linear dependence of n_{12} on τ_{12} following a step strain $\gamma = 2.5$ shown in Figure 6 confirms the stress−optic rule and yields a stress−optic coefficient $C_o = 3.07 \pm 0.03 \times 10^{-9}$ Pa^{-1}, in good agreement with published values.[14] In Figure 7, the ratio $(n_{11} - n_{22})/n_{12}$ is plotted vs time for a strain $\gamma = 2.5$. From this figure, it is evident that $(n_{11} - n_{22})/n_{12}$ is independent of time and equal to the applied strain—the optical equivalent of the Lodge−Meissner relation.[6] Hence, the results in Figures 6 and 7 confirm that there is no slip between the polymer and glass surfaces for this strain and that $\gamma\tau_{12} = \tau_{11} - \tau_{22}$. Birefringence measurements were made

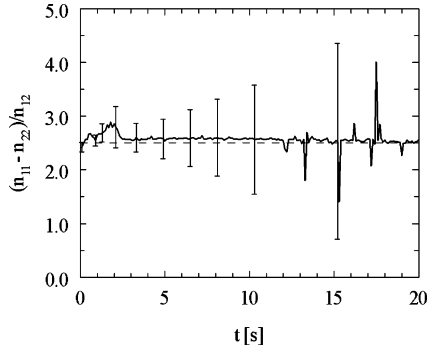

Figure 7. Refractive index tensor components $(n_{11} - n_{22})/n_{12}$ vs time for PIB131K melt following a step strain $\gamma = 2.5$ (solid curve). Consistency with dashed line confirms the optical equivalent of the Lodge−Meissner relation: $(n_{11} - n_{22})/n_{12} = \gamma = (\tau_{11} - \tau_{22})/\tau_{12}$.

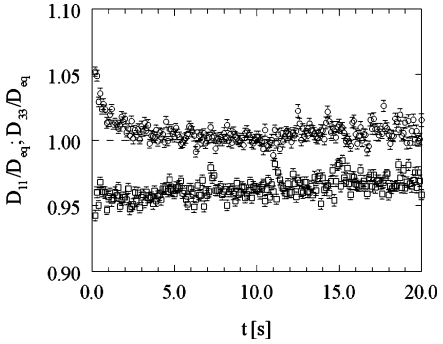

Figure 8. Thermal diffusivity tensor components for PIB131K in flow D_{11} (○) and vorticity D_{33} (□) directions normalized by D_{eq} vs time following a step strain $\gamma = 2.5$.

at larger strains, but stress-induced parasitic birefringence in the thick prisms obscured the results, making it impossible to rule out slip.

As discussed in the previous section, all reported thermal diffusivity values were obtained from independent FRS experiments made at four different grating sizes (see Figure 5). We also carefully examine each photodetector voltage trace to ensure it has the proper biexponential decay (i.e., the residuals are random in time and have a Gaussian distribution as in Figure 4) as required by eq 8.

Time-dependent values of thermal diffusivity following step strain in the flow direction D_{11} and the vorticity direction D_{33} normalized by the equilibrium thermal diffusivity D_{eq} are shown in Figure 8. In the flow direction, the thermal diffusivity is increased above the equilibrium value by ≈5% while a decrease of ≈4% is observed in thermal diffusivity measured in the vorticity direction. At long times, both D_{11} and D_{33} appear to relax to the equilibrium value. The dearth of $N_2 = \tau_{22} - \tau_{33}$ data in step strain flows makes it difficult to speculate on the explanation for the noticeably slower relaxation of D_{33}. These results are consistent with our previous study on the PIB85K melt where it was possible to achieve larger strains ($\gamma = 4, 8$) and therefore larger deviations from equilibrium.[20,21]

Figure 9 shows time-dependent values of D_{22}/D_{eq} following a step strain of $\gamma = 2.5$. The larger uncertainty in this figure, relative to D_{11} and D_{33}, is the result of needing to perform measurements at three grating vector orientations ($\alpha = 0, \pi/4, -\pi/4$) to obtain D_{22}. Thus, each symbol in Figure 9 is obtained from a total of 12 FRS experiments (three α's times four Λ's). Despite the larger uncertainty, it appears that flow reduces D_{22}

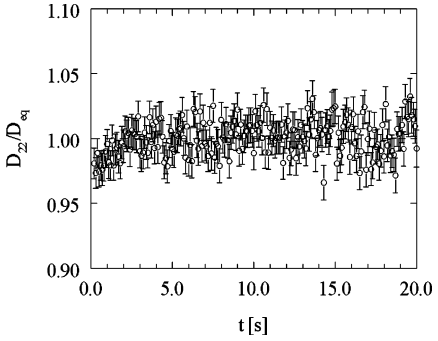

Figure 9. Thermal diffusivity tensor component for PIB131K in gradient direction D_{22} (○) normalized by D_{eq} vs time following a step strain $\gamma = 2.5$.

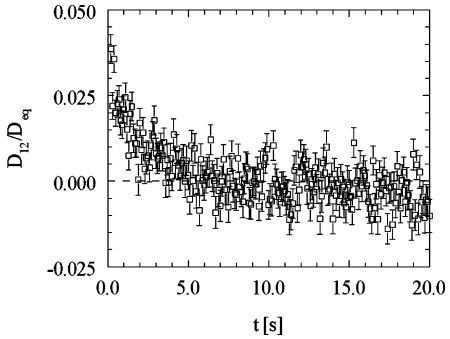

Figure 10. Shear thermal diffusivity tensor component D_{12} for PIB131K (□) normalized by D_{eq} vs time following a step strain $\gamma = 2.5$.

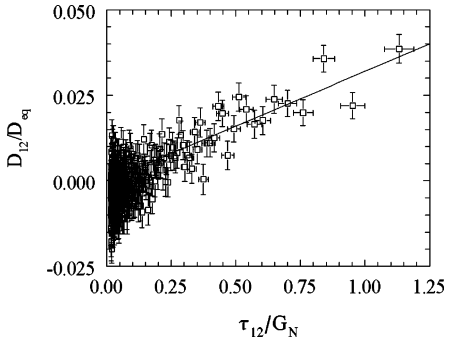

Figure 11. Test of the stress−thermal rule eq 2 following a step strain $\gamma = 2.5$ for PIB131K (symbols) showing linear dependence of D_{12} on τ_{12}. Slope of solid line yields a stress−thermal coefficient $C_t = (1.3 \pm 0.1) \times 10^{-7}$ Pa^{-1}.

relative to its value at equilibrium. From the data in Figures 8 and 9, it is clear that $D_{11} - D_{22} > 0$ and $D_{22} - D_{33} < 0$; both results are qualitatively consistent with the stress−thermal rule since it is well-established that $\tau_{11} - \tau_{22} > 0$ and $\tau_{22} - \tau_{33} < 0$ for shear flows of entangled polymer liquids.[6,7]

Normalized values of the off-diagonal, or shear, component of the thermal diffusivity tensor D_{12} vs time for $\gamma = 2.5$ are shown in Figure 10. Similar to D_{22}, the larger uncertainty in D_{12} is the result of FRS measurements made at two grating orientations. To our knowledge, these data are the first reported measurements of an off-diagonal component of the thermal diffusivity (or conductivity) tensor.[23] Immediately following the step strain, D_{12} is ≈4% of D_{eq} and decays to zero at long times. A nonzero D_{12} is qualitatively consistent with the stress−thermal rule.

Direct tests of the stress−thermal rule, eq 2, are made in Figures 11 and 12. In Figure 11, the shear component

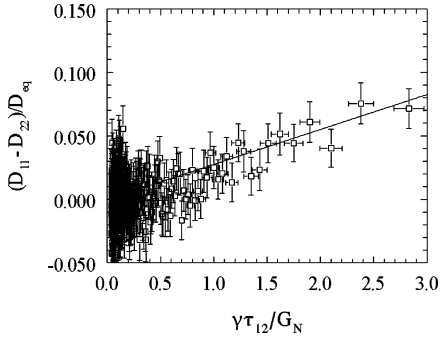

Figure 12. Test of the stress−thermal rule eq 2 following a step strain $\gamma = 2.5$ for PIB131K (symbols) showing linear dependence of $D_{11} - D_{22}$ on $\gamma\tau_{12} = \tau_{11} - \tau_{22}$. Slope of solid line yields a stress−thermal coefficient $C_t = (1.1 \pm 0.1) \times 10^{-7}$ Pa^{-1}.

of the thermal diffusivity tensor D_{12} is plotted vs the shear stress τ_{12} for $\gamma = 2.5$. Within experimental uncertainty, the data shown in this figure indicate a linear relationship between D_{12} and τ_{12} and thus support the stress−thermal rule. The slope of the solid line in Figure 11 gives the stress−thermal coefficient $C_t = (1.3 \pm 0.1) \times 10^{-7}$ Pa^{-1}. The difference between the components of the thermal diffusivity tensor in the flow and gradient directions $D_{11} - D_{22}$ is plotted vs $\gamma\tau_{12}$ for $\gamma = 2.5$ in Figure 12. According to birefringence results in Figures 6 and 7, $\gamma\tau_{12} = \tau_{11} - \tau_{22}$, so that the data in Figure 12 indicate $D_{11} - D_{22}$ is a linear function of $\tau_{11} - \tau_{22}$, in agreement with eq 2. The slope of the solid line in Figure 12 gives the stress−thermal coefficient $C_t = (1.1 \pm 0.1) \times 10^{-7}$ Pa^{-1}, which, as expected, is consistent the value obtained from the data in Figure 11.

The values of C_t found for PIB131K are consistent with values obtained in our previous studies. Data for the broad molecular weight polyisobutylene PIB85K showed $D_{11} - D_{33} \propto n_{11} - n_{33}$ and using C_o, we find $C_t = (2.0 \pm 0.2) \times 10^{-7}$ Pa^{-1}.[20,21] In a related study[28] using the same PIB85K, we recently obtained measurements of D_{12} and τ_{12} following the cessation of constant strain rate flow and find $C_t = (1.9 \pm 0.2) \times 10^{-7}$ Pa^{-1}. In an earlier study[22] on a cross-linked polysiloxane rubber in simple elongation, direct evidence for the stress−thermal rule was found, yielding $C_t = (1.3 \pm 0.1) \times 10^{-7}$ Pa^{-1}.

It is interesting to note that for polymers with completely different chemistries (polyisobutylene has a C−C backbone and polysiloxane has a Si−O backbone) the measured values of C_t have the same order of magnitude. (The stress−optic coefficients C_o for these two polymers differ by more than a factor of 10.[6]) In addition, we find that the measured value of C_t for the PIB131K melt is roughly 40% smaller than for the PIB85K melt. Interestingly, if the stress−thermal coefficient is made dimensionless with the plateau modulus G_N (= 250 kPa for PIB131K, =160 kPa for PIB85K), we find that this product is constant for the two PIBs: $G_N C_t = 0.030$. For the cross-linked silicone rubber (G_N = 200 kPa[7]), we find $G_N C_t = 0.026$.

The classical framework for predicting stress in polymers is based on elastic network models. In these theories, stress arises from the tension in chain segments trapped between entanglements (or cross-links in rubber) and is purely entropic in origin. These elastic chain segments are coarse-grained objects, and the source of this entropic tension need not actually reside in the strand itself but could also arise from interchain

interactions. Indeed, results from molecular dynamics simulations of polymer chains find that most stress arises from interchain interactions.[29,20] The success of course-grained models for entangled and cross-linked polymers, as well as experimentally observed universality in stress curve shapes, suggests that both intra- and interchain contributions to stress are adequately captured by this level of description. The proposed stress−thermal rule, which is consistent with our experiments for three polymers, is based on the same coarse-grained level of description used to predict stress. Our data also suggest that there may exist an additional universality in the value of the dimensionless stress−thermal coefficient $G_N C_t$ for flexible polymers. In other words, not only is the form of the stress−thermal rule universal, but even the parameter might be universal. This would be analogous to observing that all polymers have the same value for the plateau modulus and the same time constants.

It may be premature to suggest such a universality exists on the basis of results for only three systems. However, if true, we offer the following explanation for this observation. Note that elastic network models predict that all strands are under tension. Yet, the real network does not collapse to zero volume because there exist repulsive forces between atoms. These interactions are mostly interchain and, as we know from molecular dynamics studies, carry most of the stress. The anisotropy of these density-preserving forces give rise to anisotropic stress and may also give rise to the observed stress−thermal behavior. In other words, anisotropic orientation of entangled strands gives rise to anisotropic tension, which in turn provokes anisotropic repulsive forces between chains. These forces give rise to both stress and anisotropic thermal transport in the medium. We emphasize that these ideas are speculative, and further research on this phenomenon is clearly necessary.

Conclusions

Flow-induced anisotropic thermal conduction in a polymer melt subjected to step strain flow has been investigated experimentally. We have developed a novel version of the forced Rayleigh scattering technique to obtain the complete thermal diffusivity tensor. The reported anisotropies in thermal diffusivity (∼5% relative to equilibrium) are somewhat smaller than those found in our previous studies. This can be explained by two factors. First, the use of a nearly monodisperse polymer melt, which is more prone to exhibit wall slip, limited the present study to smaller strains. Using birefingence measurements, we were able to rule out slip for the strain level studied. Second, noise induced by the stepper motor used in the present study prevented the collection of data at times immediately after the step when the anisotropy in thermal diffusivity is largest. Despite these limitations, we were able to obtain quantitative, time-dependent measurements of four components (D_{11}, D_{22}, D_{33}, D_{12}) of the thermal diffusivity tensor.

The combination of mechanical stress measurements and birefringence measurements was used to obtain the shear stress (τ_{12}) and first normal stress difference ($\tau_{11} - \tau_{22}$). These data, in combination with D_{11}, D_{22}, and D_{12}, were used to directly test the stress−thermal rule. In both cases, the stress−thermal was satisfied, and consistent values of the stress−thermal coefficient C_t were obtained. Results from the present study and from our previous studies indicate the dimensionless stress−thermal coefficient $G_N C_t$ may be a constant for liquids composed of flexible polymers. If this is indeed the case, flow-induced anisotropic thermal conduction may be explained in terms of interchain interactions. Research in our laboratory on other polymer systems is currently underway.

Acknowledgment. The authors are grateful to the National Science Foundation for support of this study through Grant CTS-0075789 and to Jürg Hostettler of the ETH, Zürich, for his assistance in fabricating the optical flow device.

References and Notes

(1) Tucker, C. L. *Computer Modeling for Polymer Processing*; Hanser Verlag: New York, 1989.
(2) Tanner, R. I. *Engineering Rheology*, 2nd ed.; Oxford Press: Oxford, 2000.
(3) Wapperom, P.; Hulsen, M. A.; van der Zanden, J. P. P. M *Rheol. Acta* **1998** *37*, 73−88.
(4) Al-Mubaiyedh, U. A.; Sureshkumar, R.; Khomami, B. *Phys. Fluids* **1999**, *11*, 3217−3226.
(5) Rothstein, J. P.; McKinley, G. H. *Phys. Fluids* **2001**, *13*, 382−396.
(6) Bird, R. B.; Armstrong, R. C.; Hassager, O. *Dynamics of Polymeric Liquids,* 2nd ed.; Wiley-Interscience: New York, 1987; Vol. 1.
(7) Larson, R. G. *The Structure and Rheology of Complex Fluids*; Oxford University Press: Oxford, 1999.
(8) Beris, A. N.; Edwards, B. J. *Thermodynamics of Flowing Systems with Internal Microstructure*; Oxford University Press: New York, 1994.
(9) Dressler, M.; Edwards, B. J.; Öttinger, H. C. *Rheol. Acta* **1999**, *38*, 117−136.
(10) Öttinger, H. C. *Beyond Equilibrium Thermodynamics*; Wiley-Interscience: New York, 2005.
(11) van den Brule, B. H. A. A. *Rheol. Acta* **1989**, *28*, 257−266.
(12) Curtiss, C. F.; Bird, R. B. *Adv. Polym. Sci.* **1996**, *125*, 1−101.
(13) Öttinger, H. C. *Physica A* **1998**, *254*, 433−450.
(14) Janeschitz-Kriegl, H. *Polymer Melt Rheology and Flow Birefringence*; Springer-Verlag: Berlin, 1983.
(15) Fuller, G. G. *Optical Rheometry of Complex Fluids*; Oxford University Press: New York, 1995.
(16) Brown, E. F.; Burghardt, W. R.; Kahvand, H.; Venerus, D. C. *Rheol. Acta* **1995**, *34*, 221−234.
(17) Venerus, D. C.; Brown, E. F.; Burghardt, W. R. *Macromolecules* **1998**, *31*, 9206−9212.
(18) Venerus, D. C.; Zu, S.-H.; Öttinger, H. C. *J. Rheol.* **1999**, *43*, 795−813.
(19) Laup, C.; Müller, C.; Schweizer, T.; Venerus, D. C. *Rheol. Acta*, in press.
(20) Venerus, D. C.; Schieber, J. D.; Iddir, H.; Guzman, J. D.; Broerman, A. W. *Phys. Rev. Lett.* **1999**, *82*, 366−369.
(21) Iddir, H.; Venerus, D. C.; Schieber, J. D. *AIChE J.* **2000**, *46*, 610−615.
(22) Broerman, A. W.; Venerus, D. C.; Schieber, J. D. *J. Chem. Phys.* **1999**, *111*, 6965−6969.
(23) Venerus, D. C.; Schieber, J. D.; Balasubramanian, V.; Bush, K.; Smoukov, S. *Phys. Rev. Lett.* **2004**, *93*, 098301.
(24) Venerus, D. C. *J. Rheol.* **2005**, *49*, 277−295.
(25) Eichler, H. J.; Günter, P.; D. W. Pohl, D. W. *Laser-Induced Dynamic Gratings*; Springer: Berlin, 1986.
(26) Lodge, T. P. In *Applied Polymer Analysis and Characterization*; Mitchell, J., Ed.; Hanser: Berlin, 1991; Vol. II, pp 57−77.
(27) Venerus, D. C.; Schieber, J. D.; Iddir, H.; Guzman, J. D.; Broerman, *J. Polym. Sci., Polym. Phys. Ed.* **1999**, *37*, 1069−1078.
(28) Schieber, J. D.; Venerus, D. C.; Balasubramanian, V.; Bush, K.; Smoukov, S. *Proc. Natl. Acad. Sci. U.S.A.* **2004** *101*, 13142−13146.
(29) Gao, J.; Weiner, J. H. *J. Chem. Phys.* **1989**, *90*, 6749−6760.
(30) Kröger, M. *Phys. Rep.* **2004**, *390*, 453−551.

MA050827J